arXiv:1702.02106v1 [physics.flu-dyn] 1 Feb 2017

Oseen Flow in Ink Marbling

Aubrey Jaffer

Abstract

Ink marbling refers to techniques for creating intricate designs in colored inks floating on a liquid surface. If the marbling motions are executed slowly, then this layer of inks can be modeled as a two-dimensional incompressible Newtonian fluid.

In this highly constrained model many marbling techniques can be exactly represented by closed form homeomorphisms. Homeomorphisms can be composed and compute the composite mapping at any resolution. Computing homeomorphisms directly is orders of magnitude faster than finite-element methods in solving ink marbling flows.

Most marbling patterns involve drawing rakes from one side of the tank to the other; and these can be modeled by closed-form homeomorphisms. But pictorial designs for flowers and animals use short strokes of a single stylus; presented is a closed form velocity field for Oseen fluid flow and its application to creating short stroke marbling homeomorphisms.

Keywords

ink marbling; Oseen flow; Stokes flow; fluid dynamics

1. Introduction

Marbling originated in Asia as a decorative art more than 800 years ago and spread to Europe in the 1500s where it was used for endpapers and book covers.

The mathematical fascination with ink marbling is that while rakings across the tank stretch and deform the ink boundaries, they do not break or change the topology of the surface. With mechanical guides, a raking can be undone by reversing the motion of the rake to its original position. Raking is thus a physical manifestation of a homeomorphism, a continuous function between topological spaces (in this case between a topological space and itself) that has a continuous inverse function.

2. Dropping Ink

First, inks are dropped onto the surface. Consider the tank as being an infinite plane covered with a film of "empty ink" initially. The first ink drop forms a circular spot with area a. If a second drop with area b is put in the center of the first drop, then the total covered area increases from a to $a+b$. Points near the center will move from small radius to radius $\sqrt{a/\pi}$; and boundary points will move from radius $\sqrt{a/\pi}$ to radius $\sqrt{(a+b)/\pi}$.

The movements of a point on the surface do not depend on its ink color; so the motion of every point is the same as for the concentric ink-drop case. Given a point $\vec{P}$ and a new ink drop of radius r centered at $\vec{C}$, map the point $\vec{P}$ to:

$$\vec{C} + \left(\vec{P} - \vec{C}\right)\sqrt{1 + \frac{r^2}{\left\|\vec{P} - \vec{C}\right\|^2}}$$

Figure 1 shows a pattern formed by serial injection of 75 drops of random size and position. For a more complete discussion of ink-dropping see *Mathematical Marbling*[1].

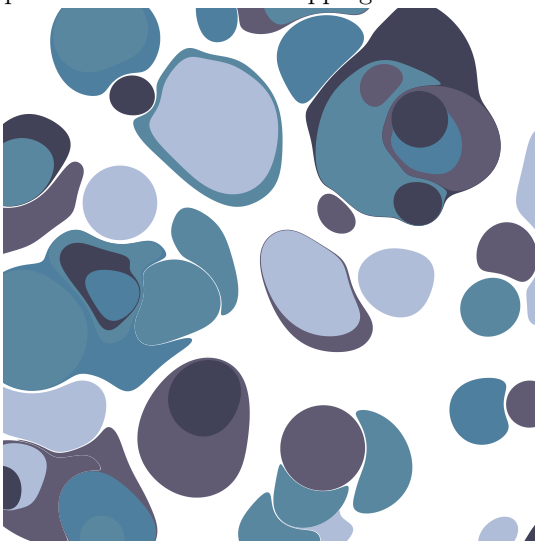

Figure 1

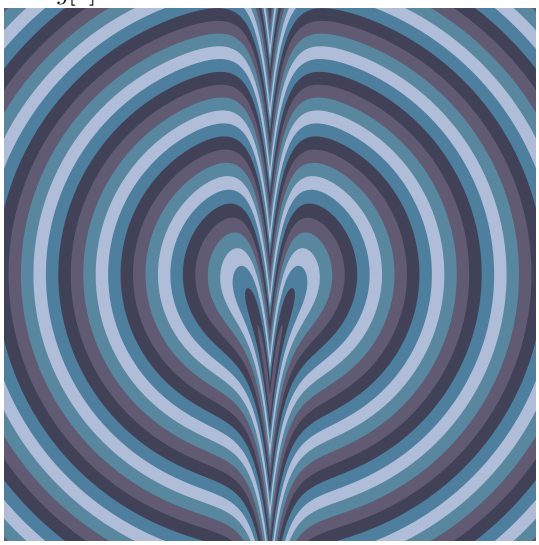

Figure 2

3. Line Deformation

Immediately adjacent to the line, particles of fluid are moved by distance λ. Because flow is laminar, flow must be uniform along the line. The friction between adjacent lamina results in exponential decrease with (normal) distance from the line. For a line on the y-axis, the displacement in the y-direction would be:

$$\lambda \exp \frac{-|x|}{L}$$

Because the displacement depends only on distance in the perpendicular direction, the displacements from parallel lines add linearly, which speeds computation of (parallel) raking homeomorphisms. Figure 2 shows a single line deformation through the center of concentric ink circles.

A line with unit direction vector $\vec{M}$ and point $\vec{B}$ on the line maps point $\vec{P}$ to:

$$\vec{P} + \lambda\vec{M} \exp \frac{\left\|\left(\vec{P} - \vec{B}\right) \times \vec{M}\right\|}{-L}$$

4. **Short Stroke**

At the 2016 Lowell Folk Festival Regina and Dan St. John (Chena River Marblers) were kind enough to let me perform an experiment on their equipment. With a marbling pattern already in the tank, I took a rod, inserted it into the tank, moved it a short distance, and withdrew it from the tank. I could then clearly see the effect of a short stroke on the ink contours floating in the tank. The bands perpendicular to the rod motion were compressed in the direction of motion and spread perpendicular to the motion to form a gentle curve. Behind the point where the rod was withdrawn the contours formed a sharp V leading to the extraction point.[1]

I repeated the experiment, but stopping the motion halfway, then resuming for the same total distance; the deformation was indistinguishable from the first stroke.

A vertical rod drawn slowly through a layer of inks floating on the surface of a liquid, one of the techniques of ink-marbling, can be treated as the motion of a circular disk in an incompressible two-dimensional liquid. Because the movement is slow, viscous forces dominate inertial forces. In the simulation of the two-dimensional Stokes model[2] shown in Figure 3, as the radius of the cylinder shrinks, the y displacements vanish. Thus the Stokes flow cannot produce the spreading I observed ahead of the motion of the rod. In the simulation of the Oseen model[3] shown in Figure 4 the streamlines are orbits displacing the y coordinates of points at any distance from disk. Although the asymmetry is subtle, the Stokes streamlines are symmetrical around the y-axis, while the Oseen streamlines are not[4].

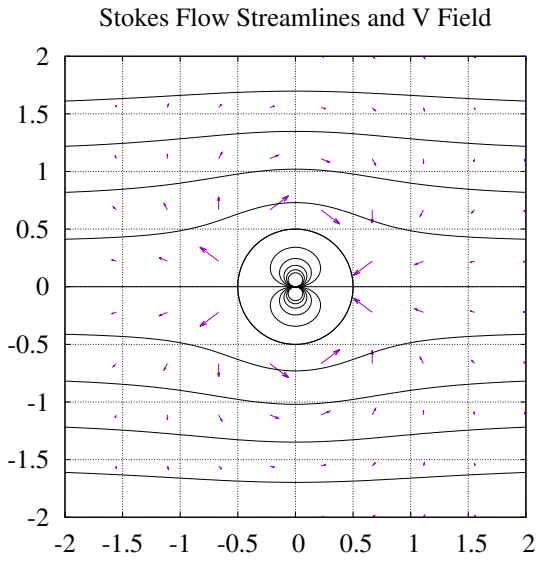

Figure 3

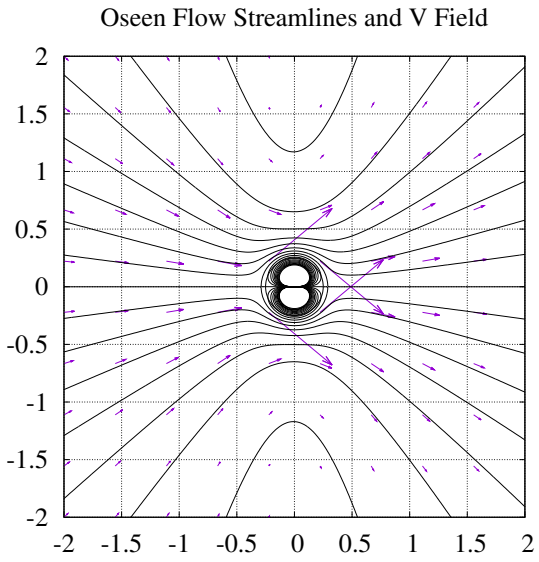

Figure 4

In "*Small Re flows,* $\epsilon = Re \ll 1$" Lagrée[5] gives a derivation of the two-dimensional Oseen formula which is composed of a near-field and far-field componenets. The near field is responsible for the flow deflecting around the cylinder, while the far field is resonsible for the wake. Because the cylinder is withdrawn at the end of the stroke, the deflection will collapse, and is not of interest for the marbling deformation. But the far-field component of the Oseen approximation results in streamlines with the potential to be more marbling-like.

[1] I was so engaged that I neglected to take a photograph.

5. Velocity Field

Because the fluid is modeled as incompressible, the divergence of the velocity field $\nabla \cdot \vec{F} = 0$. In polar coordinates:

$$\nabla \cdot \vec{F}(r,\theta) = \frac{1}{r}\frac{\partial r F_r}{\partial r} + \frac{1}{r}\frac{\partial F_\theta}{\partial \theta} = 0 \tag{1}$$

At large r values, the magnitude of the velocity vanishes.

$$\lim_{r\to\infty} \left\| \vec{F}(r,\theta) \right\| = 0 \tag{2}$$

The other boundary condition is the velocity at the origin $\vec{F}(0,0) = [U,0]$ where U is the speed. Converting this constraint to polar coordinates:

$$\vec{F}(0,\theta) = F_r(0,\theta)\hat{r} + F_\theta(0,\theta)\hat{\theta} \qquad \hat{r} = [\cos\theta, \sin\theta] \qquad \hat{\theta} = [-\sin\theta, \cos\theta] \tag{3}$$

$$U = F_r(0,\theta)\cos\theta - F_\theta(0,\theta)\sin\theta \qquad 0 = F_r(0,\theta)\sin\theta + F_\theta(0,\theta)\cos\theta$$

$$U = F_r(0,\theta)\cos\theta + F_r(0,\theta)\frac{\sin^2\theta}{\cos\theta} \qquad U = -F_\theta(0,\theta)\frac{\cos^2\theta}{\sin\theta} - F_\theta(0,\theta)\sin\theta$$

$$F_r(0,\theta) = U\cos\theta \qquad F_\theta(0,\theta) = -U\sin\theta \tag{4}$$

On the basis of the Oseen formula, it is likely that the functions $F_r(r,\theta)$ and $F_\theta(r,\theta)$ satisfying the constraints are the product of trigonometric and exponential expressions. The system characteristic length $L = \nu/U$, where ν is the dynamic viscosity of the liquid. A solution (5) is incompressible (1) and satisfies boundary conditions (2) and (4).

$$F_r(r,\theta) = U\cos\theta\exp\frac{-r}{L} \qquad F_\theta(r,\theta) = \left[\frac{r}{L} - 1\right] U\sin\theta\exp\frac{-r}{L} \tag{5}$$

Expressing (5) in Cartesian coordinates (6) according to (3) and integrating to find the stream function ψ (7):

$$r = \sqrt{x^2+y^2} \qquad F_x = U\frac{rL - y^2}{rL\exp(r/L)} \qquad F_y = U\frac{xy}{rL\exp(r/L)} \tag{6}$$

$$\psi(x,y) = \frac{Uy}{\exp(r/L)} \tag{7}$$

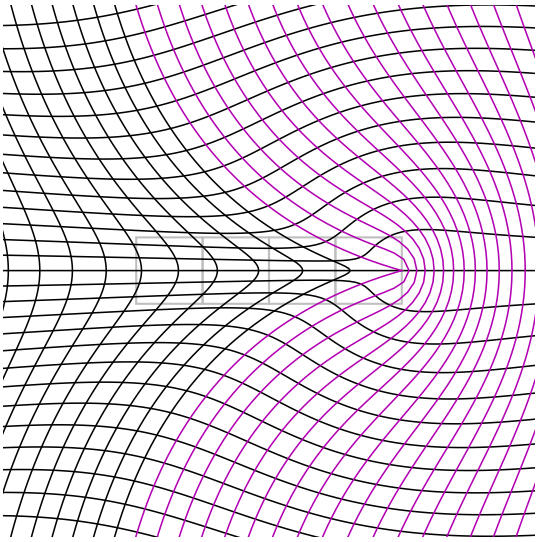

Figure 5

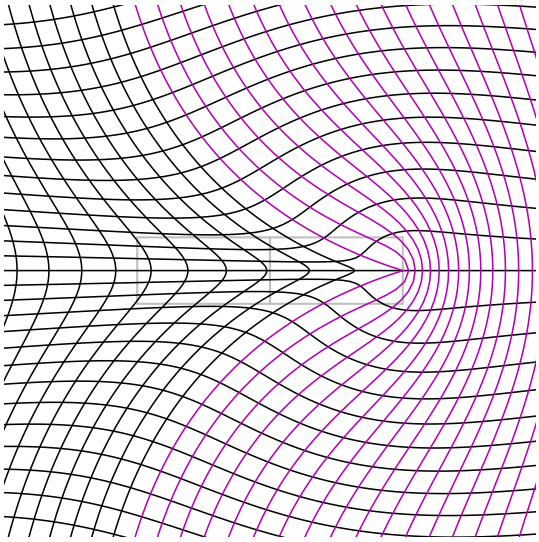

Figure 6

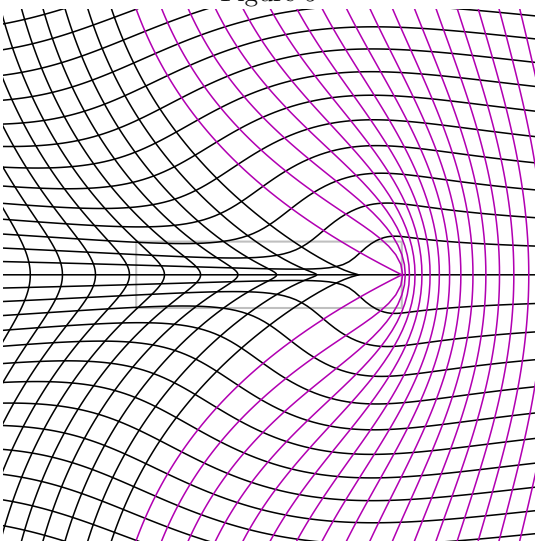

Figure 7

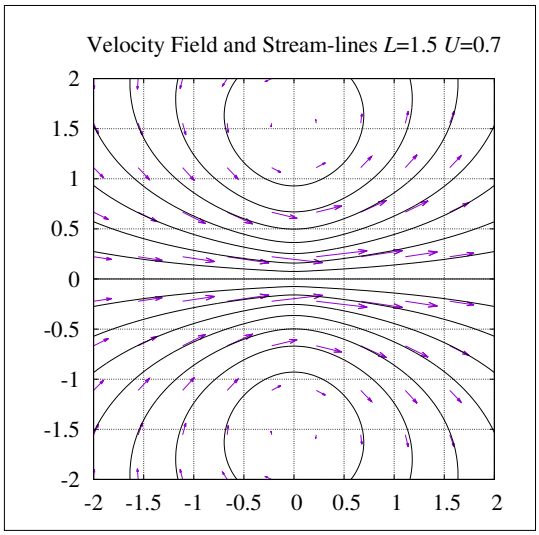

Figure 8

Figure 5 shows a displacement graph resulting from four evenly spaced applications of the velocity field to a square grid.[2] The deformation matches my description of the short stroke in the introduction; bands are compressed ahead of the stroke and a vee trails it. Figure 6 shows a displacement graph resulting from two applications of the velocity field with the same total displacement. Figure 7 shows a displacement graph resulting from one application of the velocity field to the square grid. Clearly, the area of (deformed) squares has not been preserved in Figure 7. Figure 8 shows the streamlines (contours of constant ψ values) and velocity field vectors from equations (5) in the steady-state. Because the streamlines form closed orbits, it is a rotational flow while the Stokes flow is not.

[2] The light gray boxes show the horizontal extent of each stroke; the vertical grid-lines with an initial position to the right of the beginning of the first stroke are magenta.

6. Displacement Field

So the flow velocity field is not the ultimate goal, rather the displacement after a finite time. Consider the case of a point on the horizontal line where $y = 0$. Along this line $x_f > x_0$. $t(x_f)$ is time as a function of distance, the inverse of the desired $x_f(t)$.

$$F_x(x,0) = U \exp \frac{-|x|}{L} \qquad F_y(x,0) = 0 \qquad t(x_f) = \int_{x_0}^{x_f} \frac{dx}{F_x(x,0)}$$

If $x_0 \geq 0$:

$$t(x_f) = \int_{x_0}^{x_f} \exp \frac{|x|}{L} \frac{dx}{U} = \frac{L}{U} \left[\exp \frac{x_f}{L} - \exp \frac{x_0}{L} \right]$$

$$x_f(t) = L \ln \left(\exp \frac{x_0}{L} + \frac{tU}{L} \right) \tag{8}$$

If $x_0 \leq x_f \leq 0$:

$$t(x_f) = \int_{|x_f|}^{|x_0|} \exp \frac{|x|}{L} \frac{dx}{U} = \frac{L}{U} \left[\exp \frac{|x_0|}{L} - \exp \frac{-x_f}{L} \right]$$

$$x_f(t) = -L \ln \left(\exp \frac{|x_0|}{L} - \frac{tU}{L} \right) = -L \ln (\beta) \tag{9}$$

Otherwise $x_0 \leq 0$ and $x_f \geq 0$:

$$t(x_f) = \int_0^{|x_0|} \exp \frac{|x|}{L} \frac{dx}{U} + \int_0^{x_f} \exp \frac{|x|}{L} \frac{dx}{U} = \frac{L}{U} \left[\exp \frac{|x_0|}{L} - 1 + \exp \frac{x_f}{L} - 1 \right]$$

$$x_f(t) = L \ln \left(2 - \exp \frac{|x_0|}{L} + \frac{tU}{L} \right) = L \ln (2 - \beta) \tag{10}$$

$$\beta = \exp \frac{|x_0|}{L} - \frac{tU}{L}$$

$x_0 \leq x_f \leq 0$ tests the final value of x_f which isn't yet known when trying to compute it. But the transition between $x_f(t)$ in (9) and $x_f(t)$ in (10) is $\beta = 1$; so test $\beta > 1$ instead.

When $x_0 \geq 0$ formula (8) is used. Formula (9) is used when $\beta > 1$. Otherwise formula (10) is used. Figure 9 shows the position versus time of five points on the x-axis with $L = 1.5$ and $U = 0.7$.

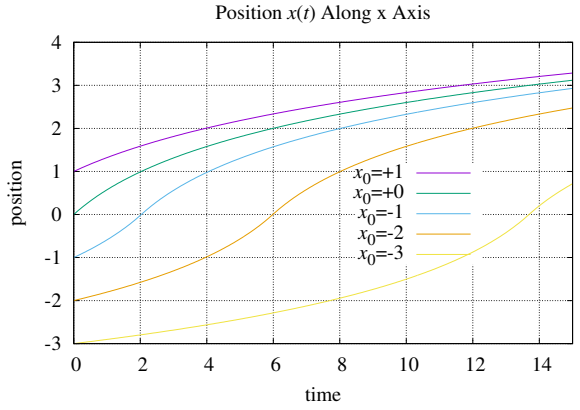

Figure 9

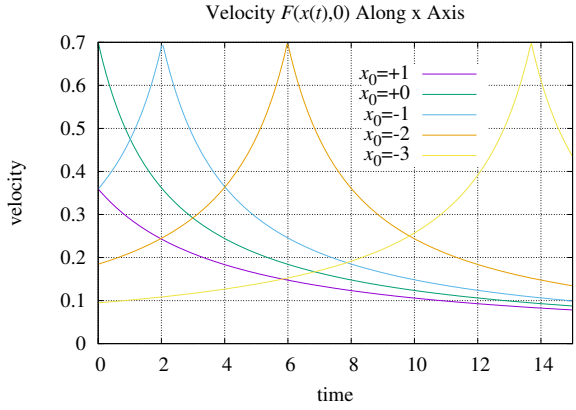

Figure 10

The derivative of $x_f(t)$ with respect to t gives the velocity as a function of x_0 and t. Figure 10 shows the velocity with $L = 1.5$ and $U = 0.7$.

$$\frac{dx_f(t)}{dt} = U \Big/ \begin{cases} tU/L + \exp|x_0|/L, & \text{if } x_0 > 0; \\ -tU/L + \exp(|x_0|/L), & \text{if } -tU/L + \exp(|x_0|/L) > 1; \\ 2 + tU/L - \exp(|x_0|/L), & \text{otherwise.} \end{cases} \tag{11}$$

Equation (11) can be simplified with $r = |x_0|$ and $\cos\theta = x_0/r$:

$$\begin{aligned} \frac{dx_f(t)}{dt} &= U \Big/ \begin{cases} \cos\theta\ tU/L + \exp(r/L), & \text{if } \cos\theta\ tU/L + \exp(r/L) > 1; \\ 2 + tU/L - \exp(r/L), & \text{otherwise.} \end{cases} \\ &= U \Big/ \left\{ 1 + \left| \exp\frac{r}{L} + \cos\theta \frac{tU}{L} - 1 \right| \right\} \end{aligned}$$

This one-dimensional case was (piece-wise) integrable becuase $t(x_f)$ is a monotonic function of a single variable. Figure 8 shows that all other streamlines are orbits. Solving for x with a constant ψ value gives a parameterization of the left $(-)$ and right $(+)$ halves of the orbits generated by (7):

$$x = \pm\sqrt{[L\ln(Uy/\psi)]^2 - y^2} \qquad y \neq 0 \tag{12}$$

The analogous approach for making $\vec{F}$ and ψ functions of time is to take the time derivative of the functional inverse of the integral of the reciprocal of the velocity as a function of y segmented at $x = 0$.

Because the orbits and their velocities are continuous, Uy/ψ along the orbits must be either greater or less than 1. Figure 11 shows that $0 < Uy/\psi \leq 1$.

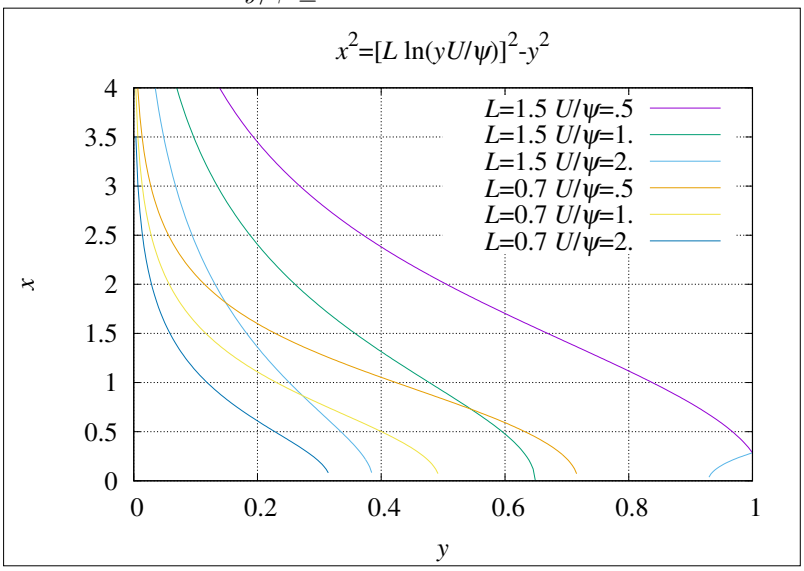

Figure 11

Let $w(y)$ be the magnitude of velocity:

$$\begin{aligned} w(y)^2 &= F_x(x_\psi(y), y)^2 + F_y(x_\psi(y), y)^2 \\ &= U^2 \frac{[L^2 + y^2]/L^2 - 2y^2 \Big/ \left[L\sqrt{L^2\ln(yU/C)^2 + y^2}\right]}{\exp\left(2\sqrt{L^2\ln(yU/C)^2 + y^2}/L\right)} \end{aligned}$$

It seems unlikely that $dy/w(y)$ will be integrable and even less likely that the displacement field will be expressible in closed form. While the vorticity of $\vec{F}$ is 0 when $y = 0$, it is non-zero away from the x-axis. This makes sense because ink-marbling develops turbulent eddies when the rod is moved too rapidly. Because this rotational system is dissipative, reversibility of strokes is not guaranteed.

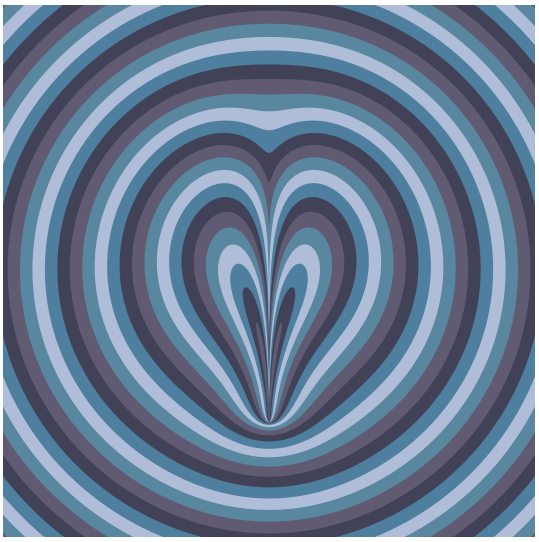

Figure 12

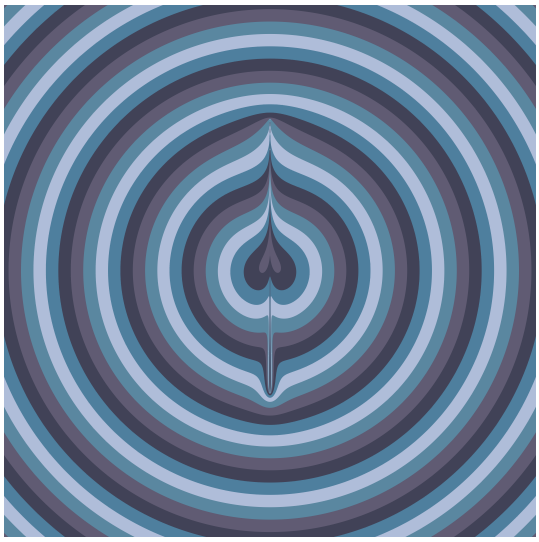

Figure 13

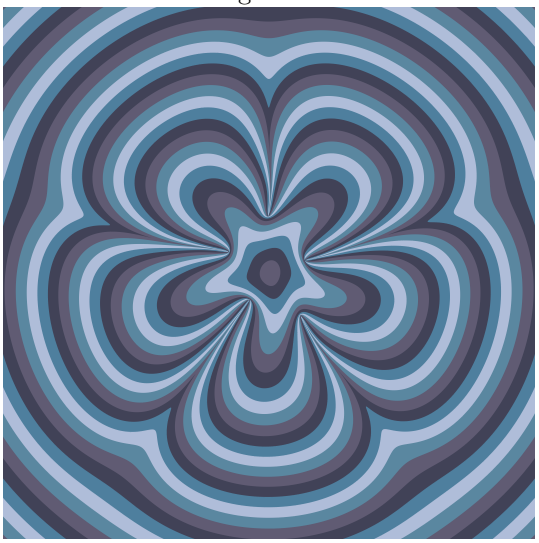

Figure 14

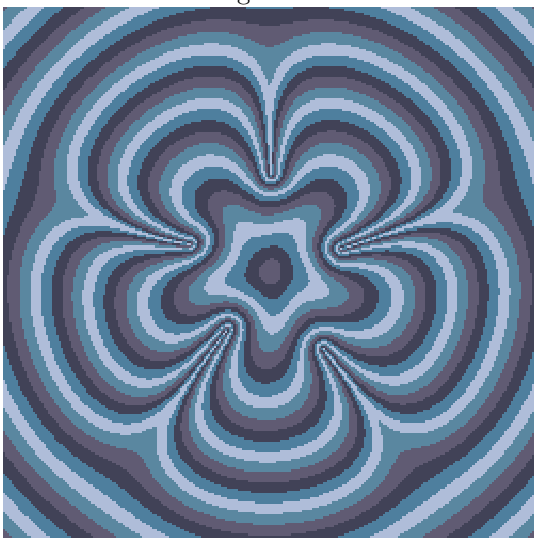

Figure 15

Figure 5 shows that with iteration, the velocity field generates a reasonable approximation to the displacement field. It was found that $\lceil tU/L \rceil = \lceil \lambda/L \rceil$ iterations produce deformations that are visually acceptable. Figure 12 shows a marbling deformation having stroke-length $\lambda = 1$ (half the height of the image) and $L = 0.15$.

With homeomorphisms we can render either by filling contours computed from the boundaries of ink-drops, or by finding the color mapped from each point of the display raster (using the inverse homeomorphism). For the exact homeomorphisms (drops, lines) the geometries rendered are the same. But the imperfect reversibility of the stroke approximation leads to geometric artifacts. Executing a stroke from $\vec{B}$ to $\vec{E}$ followed by a stroke from $\vec{E}$ to $\vec{B}$ does not completely undo the first stroke's deformation as seen in Figure 13.

Figure 14 shows a pattern with five radial strokes. The pattern is asymmetrical because the strokes were applied in the sequence 0,2,4,1,3 and each stroke affects the whole space. Figure 15 shows the raster-rendering of the same five-stroke pattern. Unlike Figure 14, the peaks of the fourth white band reach nearly all the way in.

7. Reversibility

Averaging the velocity field and the negative of the velocity field with the stroke beginning $[0, 0]$ and end $[tU, 0]$ points reversed results in a velocity field which is more nearly reversible:

$$r = \sqrt{(x - x_B)^2 + y^2} \qquad s = \sqrt{(x - x_E)^2 + y^2} \qquad tU = x_E - x_B$$

$$\begin{aligned} F_x &= \frac{U}{2}\left[\left(1 - \frac{y^2}{rL}\right)\exp\frac{-r}{L} + \left(1 - \frac{y^2}{sL}\right)\exp\frac{-s}{L}\right] \\ F_y &= \frac{U}{2}\left[\frac{(x - x_B)y}{rL}\exp\frac{-r}{L} + \frac{(x - x_E)y}{sL}\exp\frac{-s}{L}\right] \end{aligned} \tag{13}$$

Figure 16 shows a displacement graph resulting from four evenly spaced applications of the new velocity field to a square grid. Compared wth Figure 5, the point of the vee is rounded and the tail has slightly more displacement. A more rounded point is not inconsistent with the effect of a stylus having finite width. Figures 17 and 18 show displacement graphs resulting from two and one applications respectively of the velocity field with the same total displacement; both are noticeably distorted.

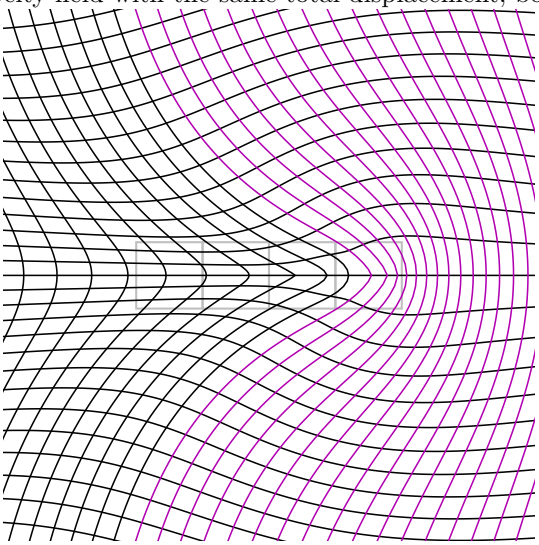

Figure 16

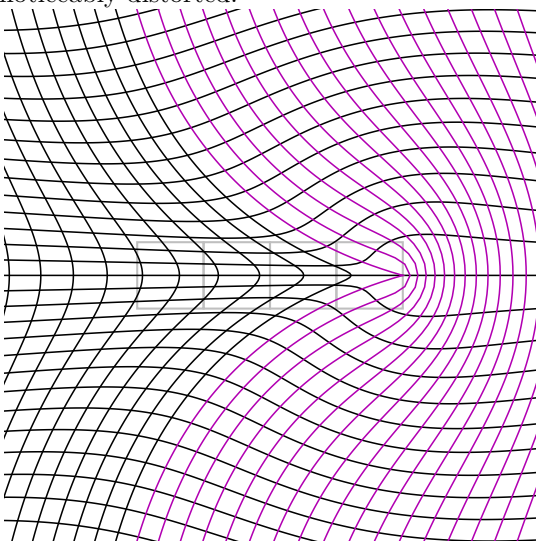

Figure 5

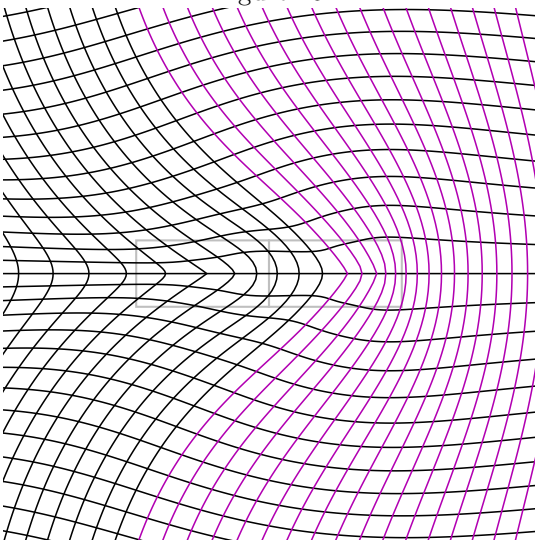

Figure 17

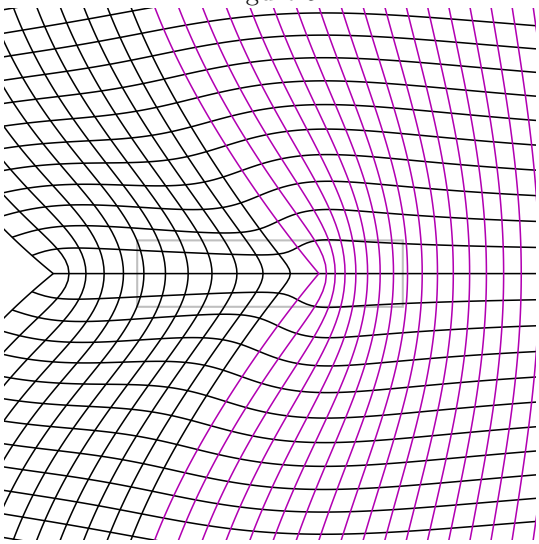

Figure 18

8. Application

This section generalizes equations (6) and (13) to work at any angle and any stroke length larger than 0.

Vector function $\vec{Q}$ maps point $\vec{P}$ to its new position as a result of a stroke from $\vec{B}$ to $\vec{E}$. For (6) the transform is:

$$\begin{aligned}
\vec{Q}\left(\vec{P},\vec{B},\vec{E},L\right) &= \vec{P} + \lambda\left[\frac{rL-y^2}{rL}\exp\frac{-r}{L}, \frac{xy}{rL}\exp\frac{-r}{L}\right] \\
\lambda &= \left\|\vec{E}-\vec{B}\right\| \\
\vec{N} &= \left(\vec{E}-\vec{B}\right)\Big/\lambda \\
\vec{C} &= \left(\vec{B}+\vec{E}\right)\Big/2 \\
r &= \left\|\vec{P}-\vec{C}\right\| \\
x &= \vec{N}\cdot\left(\vec{P}-\vec{C}\right) \\
y &= \vec{N}\times\left(\vec{P}-\vec{C}\right)
\end{aligned}$$

For (13) the transform is:

$$\begin{aligned}
\vec{Q}\left(\vec{P},\vec{B},\vec{E},L\right) &= \vec{P} + \frac{\lambda}{2}\left[\frac{rL-y^2}{rL}\exp\frac{-r}{L} + \frac{sL-y^2}{sL}\exp\frac{-s}{L}, \frac{x_B y}{rL}\exp\frac{-r}{L} + \frac{x_E y}{sL}\exp\frac{-s}{L}\right] \\
\lambda &= \left\|\vec{E}-\vec{B}\right\| \\
\vec{N} &= \left(\vec{E}-\vec{B}\right)\Big/\lambda \\
r &= \left\|\vec{P}-\vec{B}\right\| \\
s &= \left\|\vec{P}-\vec{E}\right\| \\
x_B &= \vec{N}\cdot\left(\vec{P}-\vec{B}\right) \\
x_E &= \vec{N}\cdot\left(\vec{P}-\vec{E}\right) \\
y &= \vec{N}\times\left(\vec{P}-\vec{B}\right)
\end{aligned}$$

The number of segments for the computation is $n = \left\lceil \left\|\vec{E}-\vec{B}\right\|\Big/ L \right\rceil$ and the increment vector is $\vec{I} = \left(\vec{E}-\vec{B}\right)\Big/ n$.

$$\begin{aligned}
\vec{P} &\leftarrow \vec{Q}\left(\vec{P},\vec{B},\vec{B}+\vec{I},L\right) \\
\vec{P} &\leftarrow \vec{Q}\left(\vec{P},\vec{B}+\vec{I},\vec{B}+2\vec{I},L\right) \\
&\vdots \\
\vec{P} &\leftarrow \vec{Q}\left(\vec{P},\vec{B}+(n-1)\vec{I},\vec{B}+n\vec{I},L\right)
\end{aligned} \tag{14}$$

Figure 19 shows the reversible short stroke; the point is not as sharp as Figure 12. Figure 20 shows the reversible short stroke followed by the reverse stroke; cancellation, while better than Figure 13, is not complete.

Figure 21 shows the contour-filling and Figure 22 shows the raster-rendering versions of the five radial stroke pattern. The difference between them is less than between Figures 14 and 15.

This segmented computation could be adapted to allow modeling of curved strokes.

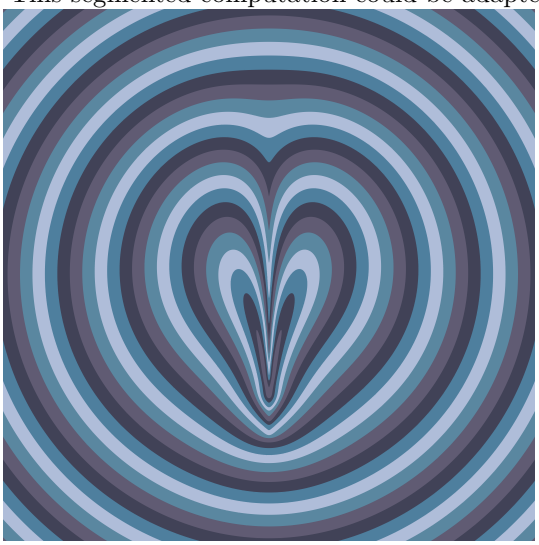

Figure 19

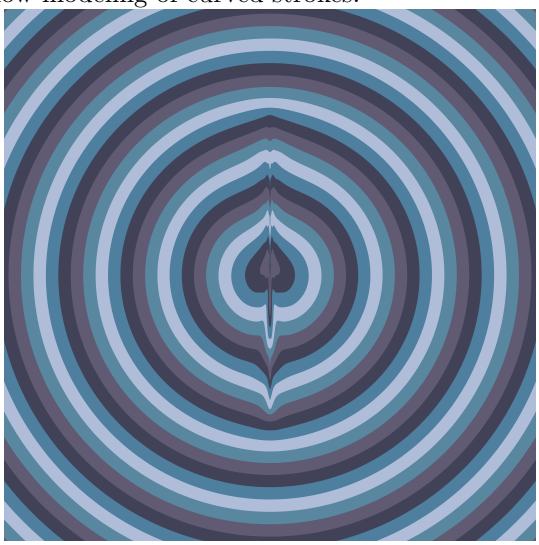

Figure 20

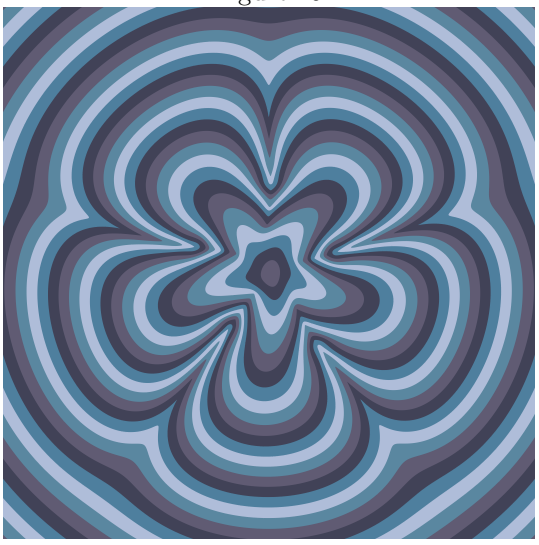

Figure 21

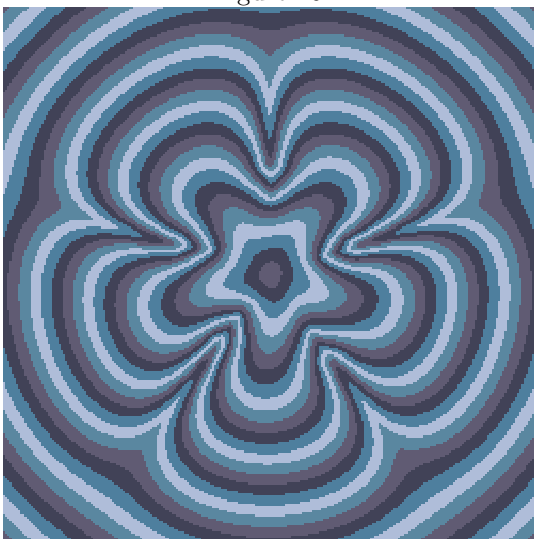

Figure 22

9. Solid Marbling

Solid Mathematical Marbling[6] introduces three-dimensional generalizations of the planar marbling primitives. How can these be adapted to finite movements? An (unbounded) line can be moved perpendicular to the line. Because there will be no flow parallel to the line, the two-dimensional calculation (14) can be used where the coordinates along the axis parallel to the line are passed through unchanged. Similar reasoning applies to a circle moved along its axis. Movement of a point is not the same as the planar case becaue there is rotational symmetry around the direction of motion; hence the 0 divergence constraint is different.

In spherical coordinates the direction of flow at the origin is along the z-axis. The angle φ around the z-axis does not change because there is no flow around the z-axis. With the fluid modeled as incompressible, the divergence of the velocity field $\nabla \cdot \vec{F} = 0$. In spherical coordinates[7]:

$$\nabla \cdot \vec{F}(r,\theta,\varphi) = \frac{1}{r^2}\frac{\partial r^2 F_r}{\partial r} + \frac{1}{r\sin\theta}\frac{\partial \sin\theta F_\theta}{\partial \theta} + \frac{1}{r\sin\theta}\frac{\partial F_\varphi}{\partial \varphi} = 0 \tag{15}$$

At large r values, the magnitude of the velocity vanishes.

$$\lim_{r\to\infty} \left\| \vec{F}(r,\theta,\varphi) \right\| = 0 \tag{16}$$

The other boundary condition is the velocity at the origin $\vec{F}(0,0,0) = [0,0,U]$ where U is the speed.

$$F_r(0,\theta,\varphi) = U\cos\theta \qquad F_\theta(0,\theta,\varphi) = -U\sin\theta \qquad F_\varphi(0,\theta,\varphi) = 0 \tag{17}$$

A solution (18) very similar to (5) is incompressible (15) and satisfies boundary conditions (16) and (17). Equations (19) shows the solution in Cartesian coordinates where $r = \sqrt{z^2+y^2+x^2}$.

$$F_r(r,\theta,\varphi) = U\cos\theta\exp\frac{-r}{L} \quad F_\theta(r,\theta,\varphi) = \left[\frac{r}{2L} - 1\right] U\sin\theta\exp\frac{-r}{L} \tag{18}$$

$$\vec{F}(r,\theta,\varphi) = F_r(r,\theta,\varphi)\hat{r} + F_\theta(r,\theta,\varphi)\hat{\theta} + F_\varphi(r,\theta,\varphi)\hat{\varphi}$$

$$\hat{r} = [\sin\theta\cos\varphi, \sin\theta\sin\varphi, \cos\theta] \quad \hat{\theta} = [\cos\theta\cos\varphi, \cos\theta\sin\varphi, -\sin\theta] \quad \hat{\varphi} = [-\sin\varphi, \cos\varphi, 0]$$

$$F_x = \frac{xzU}{2Lr}\exp\frac{-r}{L} \qquad F_y = \frac{yzU}{2Lr}\exp\frac{-r}{L} \qquad F_z = \left[2Lr - y^2 - x^2\right]\frac{U}{2Lr}\exp\frac{-r}{L} \tag{19}$$

References

[1] Shufang Lu, A. Jaffer, Xiaogang Jin, Hanli Zhao, and Xiaoyang Mao. Mathematical marbling. *IEEE Computer Graphics and Applications*, 32(6):26–35, 2012.

[2] Wikipedia. Potential flow around a circular cylinder — wikipedia, the free encyclopedia, 2016. [Online; accessed 30-October-2016].

[3] Wikipedia. Oseen equations — wikipedia, the free encyclopedia, 2016. [Online; accessed 15-October-2016].

[4] Hermann Schlichting, Klaus Gersten, Egon Collaborateur. Krause, Herbert Collaborateur. Oertel, and Katherine Mayes. *Boundary-layer theory.* Springer, Berlin, Heidelberg, Paris, 2000. Corrected printing 2003.

[5] P.Y. Lagrée. Small re flows, $\epsilon = re \ll 1$, 2015.

[6] Shufang Lu, Xiaogang Jin, Aubrey Jaffer, Fei Gao, and Xiaoyang Mao. Solid mathematical marbling. *IEEE Computer Graphics and Applications*, in press.

[7] Wikipedia. Spherical coordinate system — wikipedia, the free encyclopedia, 2016. [Online; accessed 19-December-2016].